12.1

COMPUTATION OF THE EFFECTS OF INHOMOGENEOUS CLOUDS ON RETRIEVAL OF REMOTELY SENSED PROPERTIES

Lin H. Chambers *
NASA Langley Research Center, Hampton, VA

1. INTRODUCTION

Current and future earth observation programs depend on satellite measurements of radiance to retrieve the properties of clouds on a global basis. At present, this retrieval is made assuming that the clouds in the instrument field of view are plane parallel and independent of adjacent pixels. While this assumption is known to be false except in very limited cases, its impact can be evaluated, and if possible corrected, based on emerging theoretical techniques.

In this study, the Spherical Harmonic Discrete Ordinate Method (SHDOM, Evans, 1996) has been used to assess the sensitivity of the retrieval to a variety of cloud parameters. SHDOM allows the plane parallel assumption to be relaxed and makes 2D and even 3D radiative solutions practical. A previous study (Chambers et al., 1996) assessed the effect of horizontal inhomogeneity in 45 LANDSAT scenes of boundary layer clouds over ocean. The four scenes studied here represent overcast, broken, scattered and strongly thermally forced cloud fields and are used to perform sensitivity studies to a wider variety of parameters. Comparisons are made at three solar zenith angles (θ_0 = 0, 49, and 63°) to avoid ambiguity in the results due to solar zenith angle.

2. REFERENCE AND PERTURBED CLOUD FIELDS

The reference cloud condition is that used in Chambers et al. (1996) and has the following assumptions: zero surface reflectance, an empirical relation (Minnis et al., 1992) for cloud physical thickness, no gas absorption, constant 10 μm cloud water droplet effective radius and uniform extinction with height; all with 2D radiative transport. All calculations assume conservative scattering at 0.83 μm, and a flat cloud top. A Mie phase function is used for a gamma distribution of particles with effective variance 0.1. Only the atmospheric layer containing cloud is included in the calculation. A retrieval curve for optical depth as a function of reflectance is generated for the reference case. The assumptions are then relaxed one at a time, and the retrieved optical depth is compared to that in the reference case. Unless otherwise noted, calculations are made on 20 randomly placed horizontal scan line samples from each scene (see Chambers et al., 1996 for details). While radiative smoothing may affect the LANDSAT data at the pixel scale, it has been shown (Chambers et al., 1996) to have little effect on results averaged over a scan line sample as in this paper.

2.1 Surface Reflectance

A constant surface reflectance of 6%, representative of ocean properties, was added. For this case alone, a new retrieval curve was generated including the surface reflectance.

2.2 Cloud Thickness

The relation for cloud thickness in the reference case was developed (Minnis et al. 1992) using data on a 30 km scale. Its application at the LANDSAT 28.5 m pixel scale is questionable. To assess the sensitivity to this relation, solutions were run using constant thickness clouds: 200 m for broken and scattered cloud fields, 300 m for overcast, and 750 m for strong thermal forcing.

2.3 Gas Absorption

Gas absorption effects were added using the correlated k-distribution technique of Kratz (1995). Six k-values for water vapor in AVHRR channel 2, Interval 3 (0.78-0.91 μm) are used to model the effect of absorption on a multi-channel instrument.

2.4 Variable Particle Size

A particle size variation as a function of height within the cloud was introduced. Based on thermodynamic principles (e.g., Rogers and Yau, 1989; or Considine et al., 1996) a linear variation of liquid water content with height is used. Following Martin et al. (1994) effective radius is:

$$r_e = \left(\frac{3L}{4\pi\rho_w k N_{TOT}}\right)^{1/3} \qquad (1)$$

where L is the mass of liquid water per unit volume of air, ρ_w is the density of liquid water, and N_{TOT} is the total

* *Corresponding author address*: Lin H. Chambers, Atmospheric Sciences Division, Mail Stop 420, NASA Langley Research Center, Hampton, Virginia 23681-0001; e-mail <l.h.chambers@larc.nasa.gov>.

droplet concentration. k is set to one in each cloud column.

Assuming the extinction efficiency factor equals 2, the optical depth can be estimated (Nakajima and King 1990) from:

$$\tau \approx \frac{3}{2\rho_w}\int_0^{\Delta z}\frac{L(z')}{r_e(z')}dz' \qquad (2)$$

Substituting $L=Az$ and Eq. (1) for r_e gives

$$\tau \approx \frac{3}{10}\left(\frac{3A}{\rho_w}\right)^{2/3}(4\pi N_{TOT})^{1/3}\Delta z^{5/3} \qquad (3)$$

where Δz is the cloud thickness in m. The constant A describing the liquid water content variation can be calculated from thermodynamics. A=0.0021 g/m^4 is found to be consistent with the relation for Δz (Minnis et al. 1992), remarkably close to the value used by Austin et al. (1995). N_{TOT} can also be constrained to maintain consistency with the Minnis relation. This yields values of N_{TOT} (cm^{-3}) which are entirely consistent with the range in continental air masses reported by Martin et al. (1994), but vary from column to column within a cloud. Future results will assume a constant value of N_{TOT}.

The extinction is now also a function of height within the cloud, and can be calculated from:

$$\beta_e(z) = 2\pi(0.001)[r_e(z)]^2 N_{TOT} \qquad (4)$$

With N_{TOT} in cm^{-3} and r_e in μm, this gives β_e in km^{-1}. An example of the variation of r_e in a thin scattered cloud field is given in Fig. 1. In the thickest clouds in this study, the maximum r_e at cloud top is 10.86 μm.

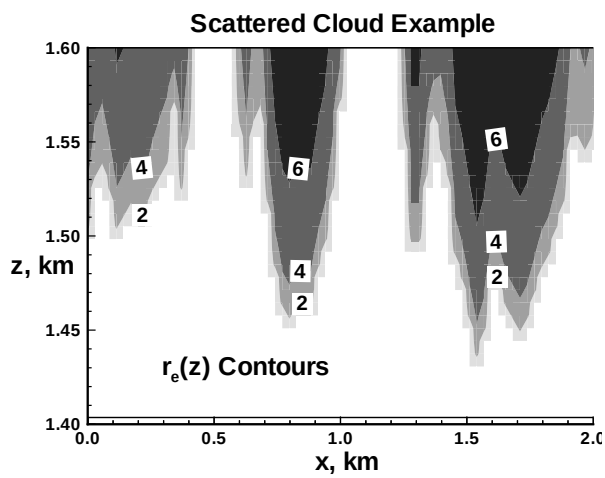

Figure 1. Sample of variation of effective radius in scattered cloud field.

The scattering phase function is highly forward-peaked for r_e=10 μm. The forward peak drops one and a half orders of magnitude as r_e decreases to 2 μm. The backward peak is insensitive to particle size in this range, but at other angles the phase function increases by up to half an order of magnitude.

2.5 Three-Dimensional Transport

A single 80 by 80 pixel sample from each scene has been computed with full 3D radiative transfer. This single calculation takes about the same amount of CPU time as the 2D solution of 20 scan line samples. Each horizontal scan line segment within the 3D sample is then treated as a separate scan to generate results comparable to those for the 2D runs.

3. RESULTS AND DISCUSSION

Results are presented as $\tau_{retrieved}$ versus τ_{input}. In most cases, horizontal transport effects cause a change in both the slope and offset of the relationship between the two. An example is shown in Fig. 2 for the scattered cloud field and the reference cloud conditions. Each point on this figure is the average optical depth for one scan line sample from the scene.

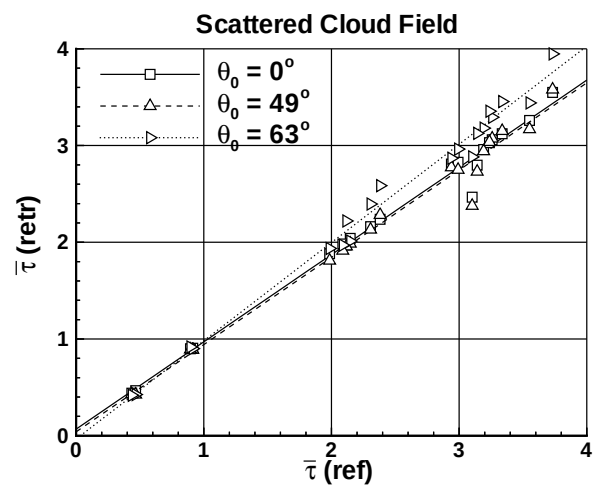

Figure 2. Example of retrieved versus reference (input) optical depth.

3.1 Overcast Cloud Field

Scan line samples have mean cloud optical depths between about 7 and 20. The single sample in the 3D case covers the range from 4 to 10. The optical depth retrieval for the various cases is summarized in Table 1. The reference overcast case has about 5 percent error in the retrieval of τ. This result is not terribly sensitive to the parameters varied in this study for overhead sun, but becomes more sensitive as the solar zenith angle increases. At θ_0=0°, the result is most sensitive to 3D transport. At low sun, it is most sensitive to cloud thickness and variable r_e. Surface reflectance has essentially no effect on this case. Assuming constant cloud thickness tends to increase the retrieval for larger τ, even beyond the reference value. Adding gas absorption

leads to a decrease in retrieved τ over the entire range. Inclusion of variable effective radius slightly decreases τ_{retr} at high sun, and increases it at low sun. Smaller particles appear at cloud top than in the reference case, and these result in more energy reflected at low sun angles. Using 3D transport has only a minor effect in the overcast case, as might be expected.

Table 1 Summary of Optical Depth Retrieval Sensitivity for Overcast Cloud Field

	$\theta_0=0^o$		$\theta_0=49^o$		$\theta_0=63^o$	
	Slope	Intercept	Slope	Intercept	Slope	Intercept
Ideal	1.	0.	1.	0.	1.	0.
Reference	0.945	0.37	0.944	0.26	0.952	0.23
Surface Refl.	+0.001	-0.02	+0.002	-0.06	+0.004	-0.08
Constant Δz	+0.005	+0.01	+0.048	-0.17	+0.122	-0.69
Gas absorption	-0.026	+0.03	-0.012	+0.01	-0.016	+0.04
Variable r_e	-0.002	-0.28	+0.053	+0.36	+0.067	+0.38
3D Transport	-0.055	+0.44	-0.057	+0.55	-0.039	+0.53

3.2 Broken Cloud Field

Scan line samples have mean optical depths between about 0.5 and 25. The cloud fraction in this case is 41 percent. The 3D sample covers optical depths from 0 to 5. Table 2 summarizes the retrieval sensitivity for this cloud type. The retrieval error in the reference case is about 10 percent at high sun, decreasing to 3 percent at low sun. As expected, these results are more sensitive to the parameter variations. At high sun 3D transport yields the most variation, while at low sun the slope is most sensitive to 3D transport and the intercept to variable effective radius. Adding surface reflectance has a small effect in this case, which increases with τ. The effect of constant cloud thickness increases with solar zenith angle, as more of the incoming sunlight is intercepted by the cloud sides. Adding gas absorption slightly reduces τ_{retr} but has little effect in this thin cloud. Including a variable effective radius does alter the result, particularly for low sun angles where the incoming sunlight directly reaches the smaller cloud particles in the lower parts of the clouds, and where the smaller particles at cloud top - particularly in cloud edges - reflect more radiation into the viewing direction. The effects of 3D transport are relatively small, but the single sample chosen in this case is not particularly representative of the cloud field as a whole.

Table 2 Summary of Optical Depth Retrieval Sensitivity for Broken Cloud Fields

	$\theta_0=0^o$		$\theta_0=49^o$		$\theta_0=63^o$	
	Slope	Intercept	Slope	Intercept	Slope	Intercept
Ideal	1.	0.	1.	0.	1.	0.
Reference	0.893	0.07	0.921	-0.02	0.970	0.04
Surface Refl.	-0.001	-0.03	+0.013	-0.03	+0.022	-0.15
Constant Δz	+0.031	-0.12	+0.037	-0.01	+0.075	+0.17
Gas absorption	-0.021	+0.03	-0.013	+0.01	-0.005	-0.03
Variable r_e	+0.007	+0.01	+0.076	+0.41	+0.098	+0.40
3D Transport	-0.044	+0.25	-0.081	+0.33	-0.111	+0.23

3.3 Scattered Cloud Field

Scan line samples have mean optical depths

between about 0.5 and 4. The cloud fraction in this scene is 29 percent. The 3D sample τ ranges from 0.5 to 3.6. Retrieval statistics are summarized in Table 3. The sensitivity to parameter variations increases further for the more scattered cloud fields. At high sun the results are most sensitive to variable r_e, while at low sun the slope is most sensitive to variable r_e and the intercept to 3D transport. Surface reflectance affects the slope of the retrieval mainly due to threshold issues for small cloud optical depth. Assuming constant thickness clouds again increases the retrieval error, due to over-emphasis of cloud sides. As in the broken case, gas absorption has little impact over this small cloud thickness but results in a slight under-retrieval of τ. Variable effective radius has a large effect, again due to incoming sunlight directly reaching small particles near the bottom of the clouds and at the edges of cloud tops. Effects of 3D transport are generally to smooth out the optical depth field, with τ_{retr} higher than τ_{ref} for small τ and the reverse for larger τ.

Table 3 Summary of Optical Depth Retrieval Sensitivity for Scattered Cloud Fields

	$\theta_0=0^o$		$\theta_0=49^o$		$\theta_0=63^o$	
	Slope	Intercept	Slope	Intercept	Slope	Intercept
Ideal	1.	0.	1.	0.	1.	0.
Reference	0.902	0.07	0.902	0.04	1.015	-0.03
Surface Refl.	-0.007	-0.01	+0.026	+0.05	-0.093	+0.21
Constant Δz	-0.014	-0.04	+0.008	-0.07	+0.142	-0.19
Gas absorption	+0.038	-0.08	+0.000	-0.04	-0.020	-0.01
Variable r_e	+0.155	-0.25	+0.288	-0.10	+0.299	-0.11
3D Transport	-0.090	+0.23	-0.132	+0.28	-0.187	+0.29

3.4 Strongly Thermally Forced Cloud Field

Scan line samples have mean optical depths between about 1 and 24. (Pixel optical depths in this case range up to 100.) The cloud fraction in this scene is 59 percent. The sensitivity of these results is comparable to those for the scattered cloud field. At high sun the results are most sensitive to variable effective radius, while at low sun the slope responds most to cloud thickness and the intercept to variable r_e. The sensitivity to cloud thickness results from interception of incoming sunlight by cloud sides, which are overemphasized by the assumption of constant Δz. This effect is strongest in this case, because the cloud is quite thick. Surface reflectance affects the results only when the sun is not overhead, and leads to an increase in retrieved τ. Gas absorption is still a small effect in this relatively thick cloud. The effect of variable particle size is to increase τ_{retr} throughout, again due to the presence of smaller particles in cloud edges and at cloud top.

Table 4 Summary of Optical Depth Retrieval Sensitivity for Strongly Thermally Forced Cloud

	$\theta_0=0^o$		$\theta_0=49^o$		$\theta_0=63^o$	
	Slope	Intercept	Slope	Intercept	Slope	Intercept
Ideal	1.	0.	1.	0.	1.	0.
Reference	0.448	1.33	0.734	0.37	1.17	-0.27
Surface Refl.	+0.004	-0.04	+0.040	+0.13	+0.028	+0.19
Constant Δz	-0.076	-0.25	+0.159	-0.73	+0.284	+0.41
Gas absorption	+0.008	+0.04	+0.005	+0.06	+0.017	+0.03
Variable r_e	+0.088	-0.30	+0.181	+0.32	+0.101	+0.75
3D Transport						

The 3D solution in this case is the most computationally intensive in this paper, requiring about 150 hours of CPU time and nearly 1 GB of run-time memory. Final results were not available at press time.

4. CONCLUSIONS

A study has been conducted of the sensitivity of horizontal radiative transport to variations in a number of cloud field parameters. The results suggest that properly modeling the variation of effective radius in the cloud and the thickness of the cloud column are important in studies of this problem. Allowing full 3D radiative transport is also important, but always results in a reduction in retrieved optical depth relative to the 2D solution. Thus it might be amenable to parameterization, rather than requiring a CPU intensive 3D solution in every case.

5. REFERENCES

Austin, P., Y. Wang, R. Pincus, and V. Kujala, Precipitation in Stratocumulus Clouds: Observational Modeling and Results, *J. Atmos. Sci.*, Vol. 52, No. 13, pp. 2329-2352.

Chambers, L. H., B. A. Wielicki, and K. F. Evans, On the accuracy of the independent pixel approximation for satellite estimates of oceanic boundary layer cloud optical depth, revision submitted to *J. Geophys. Res.*, September, 1996.

Considine, G., J. A. Curry, and B. A. Wielicki, Modeling Cloud Fraction and Horizontal Variability in Boundary Layer Clouds, submitted to *J. Geophys. Res.*, April 1996.

Evans, K. F., The Spherical Harmonics Discrete Ordinate Method for Three-Dimensional Atmospheric Radiative Transfer, submitted to *J. Atmos. Sci.*, 1996.

Kratz, D. P., The Correlated k-Distribution Technique as Applied to the AVHRR Channels, *J. Quant. Spectrosc. Radiat. Transfer*, Vol. 53, No. 5, 1995, pp. 501-517.

Martin, G. M., D. W. Johnson, and A. Spice, The Measurement and Parameterization of Effective Radius of Droplets in Warm Stratocumulus Clouds, *J. Atmos. Sci.*, Vol. 51, No. 13, pp. 1823-1842, 1 July 1994.

Minnis, P., P. W. Heck, D. F. Young, C. W. Fairall, and B. J. Snider, Stratocumulus Cloud Properties Derived from Simultaneous Satellite and Island-Based Instrumentation during FIRE, *J. Appl. Meteor.*, Vol. 31, No. 4, April 1992, pp. 317-339.

Nakajima, T., and M. D. King, Determination of the Optical Thickness and Effective Particle Radius of Clouds from Reflected Solar Radiation Measurements. Part I: Theory, *J. Atmos. Sci.*, Vol. 47, No. 15, Aug. 1990, pp. 1878-1893.

Rogers, R. R. and M. K. Yau, A Short Course in Cloud Physics, 3rd ed., Pergamon Press, 1989.